encit 2020

ABCM Associação Brasileira de Engenharia e Ciências Mecânicas

18th Brazilian Congress of Thermal Sciences and Engineering
November 16-20, 2020 (Online)

ENC-2020-0297
Thermodynamic analysis of a solar chimney using meteorological data from Rio de Janeiro and Seropédica cities.

Erick Sabino de Oliveira
José Luiz Zanon Zotin
Centro Federal de Educação tecnológica CEFET/RJ - Uned Itaguaí - Departamento de Engeharia Mecânica, Rod. Gov. Mário Covas, s/n - Santana, Itaguaí - RJ, 23812-101
ericksabinooliveira1@gmail.com, jose.zotin@cefet-rj.br

Abstract. *Ventilation is a process that guarantees the control of contaminants, an improved thermal comfort, and an adequate air supply for people, generally, using mechanical blowers or exhaust fans powered by electrical energy. A solar chimney is a device that consists of a closed conduit with a solar energy absorber on, at least, one of its faces. This absorptive material is responsible for heating the air inside the conduit generating an airflow due to natural convection. The present study investigates a solar chimney as an alternative element for indoor ventilation for Rio de Janeiro and Seropédica Cities. The study was performed from data collected at 5 weather stations located within these cities, with hourly measurements between July/18 and July/19. A thermodynamic analysis was carried out to estimate the airflow generated by the chimney for nine different inclined positions, which were tested with real climate data from these cities. In general, inclinations between* 60° *and* 70° *were the ones that provided the highest flow to the solar chimney regardless of the time or month analyzed.*

Keywords: *Solar Chimney, Solar energy, Ventilation, Thermal Comfort*

1. INTRODUCTION

An important step in building projects deals with the internal circulation of air, which must be maintained with a certain quality inside all rooms to ensure the control of pollutants as well as reducing the thermal load required for the air conditioning system as Clezar and Nogueira (1999) argues. According to Freixanet *et al.* (2004), the use of natural wind currents in the urban environment is not always possible, since the presence of buildings tends to increase the thickness of the atmospheric boundary layer and, consequently, reducing the wind speed throughout this region.

Thus, a solution to generate a natural airflow inside buildings is the use of solar chimneys. Ong (2003) defines the solar chimney as a channel where one or more faces are built with a transparent material to stimulate the greenhouse effect, while at least one of the faces must be built with high absorptive material. This material will heat the air close to the face, generating an airflow due to the natural convection that will exist inside the chimney. In addition, the chimney outlet must be directed out of the ventilated room to promote air renewal.

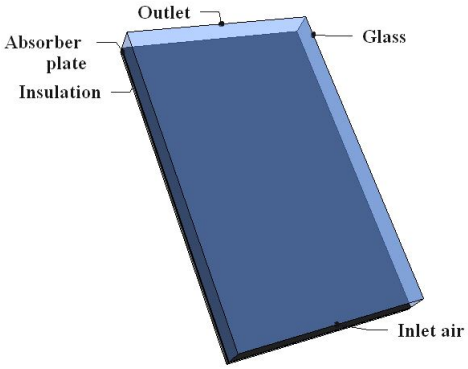

Figure 1: Schematic of a solar chimney

Despite the vast current literature on solar chimneys, there is no consensus about the optimal geometry, position, or tilt angle. With regard to the tilt angle, it is known that the airflow is as higher as the inclination. On the other hand, a high tilt angle decreases the solar energy received on the solar plate. The chimney location as well as the period of the year

in which the measurement is being made can also impact the solar radiation that reaches the chimney wall, also changing the generated airflow. Due to some researchers focused on finding the optimum tilt angle, Chen *et al.* (2003) suggests that the airflow is increased by almost 45% if the chimney is tilted to $45°$ in comparison with a vertical chimney. The study of Sakonidou *et al.* (2008) found a range between $65°$ and $76°$ to be the optimum inclination at Serres, Greece, located at latitude $41°$ N. With the same purpose, it was calculated by Bassiouny and Korah (2009) a range between $45°$ and $75°$ for latitude $28,4°$. Mathur *et al.* (2006b) carried out a study on Jaipur city, India, at latitude $26,9°$ N and found a $45°$ to be the optimum inclination. With this tilt angle, they calculated an airflow 10% higher in comparison with a tilt angle of $30°$ or $60°$. The same value for the inclination was found by Jianliu and Weihua (2013) at Nanjing, China, latitude $32°$.

Mathur *et al.* (2006a) showed that increasing the gap between the absorber and the glass increased the solar chimney's airflow. More recently, Hung *et al.* (2017) found a 5:1 ratio for the length in relation to the gap of the system. About the solar chimney's height, the higher the solar chimney the higher the airflow, due to the buoyancy effect and the constant heating. The present study focused on performing a thermodynamic analysis from real climatic data to assess the best solar chimneys inclination. Hence, it was collected hourly data from five weather station located at Rio de Janeiro and Seropédica city.

2. METHODOLOGY

At first, it was collected data from INMET (2019) for Rio de Janeiro and Seropédica cities. These data contain hourly measurements from July/18 to July/19 for the five weather stations located in these cities. The stations' positions, the number of collected measurements, and the radiations averages at midday are shown in Tab. 1. The first four weather stations listed in Tab. 1 are located within the city of Rio de Janeiro.

Table 1: Stations coordinates and average radiation at midday

Weather Station	Latitude	Longitude	Collected data	Avg radiation at midday
Copacabana	-22.98	-43.19	8741	692.06
Jacarepaguá	-22.93	-43.40	8747	633.99
Vila Militar	-22.86	-43.41	8743	626.99
Marambaia	-23.05	-43.59	8722	658.12
Seropédica	-22.75	-43.68	8703	647.17

To evaluate the best inclination of the solar chimney, each measurement was simulated under 9 different inclinations, according to the method described in section 2.1. Afterward, the solar chimney energy balance is quantified and for each measurement, the functioning of the solar chimney was simulated and the temperature and flow values were taken by repeated iterations until the convergence of the results.

2.1 Irradiation on inclined surfaces

To perform the total radiation estimate on an inclined surface, the Liu e Jordan *Apud* Duffie and Beckman (2013) model will be considered, which is given by:

$$I_t = I_b R_b + \frac{1}{2} I_d(\cos\beta + 1) + \frac{1}{2} I \rho_g (1 - \cos\beta) \tag{1}$$

where I_b, I_d and I, are respectively the beam radiation, the diffuse radiation and the global radiation. β is the tilt angle, ρ_g is the albedo coefficient and R_b represents a geometric factor defined as the ratio between beam radiation on the inclined plane and radiation on the horizontal plane. The beam and diffuse radiation can be taken from Erbs *et al.* (1982), shown on Eq. (2), where K_t is the clearness index, which means the relationship between the global and extraterrestrial radiation. The present study assumes $\rho_g = 0.2$ and azimuth equals to $180°$.

$$\frac{I_d}{I} = \begin{cases} 1 - 0.09K_t, & \text{se } K_t \leq 0.22 \\ 0.9511 - 0.1604K_t + 4.388K_t^2 - 16.638K_t^3 + 12.336K_t^4, & \text{se } 0.22 < K_t \leq 0.80 \\ 0.165, & \text{se } K_t > 0.8 \end{cases} \tag{2}$$

To estimate the extraterrestrial radiation, shown in Eq. (3a), the Muneer (2007) method was used, where n represents the day's number and α the solar elevation, shown in Eq. (3b).

$$I_o = 1367(1 + 0.033\cos 0.0172024n)\sin\alpha \tag{3a}$$

$$\alpha = \arcsin\left(-\cos\phi\cos\delta\cos\omega - 180 + \sin\phi\sin\delta\right) \tag{3b}$$

The R_b factor can be calculated as a function of solar declination δ, latitude ϕ, hour angle ω.

$$R_b = \frac{\cos(\phi+\beta)\cos\delta\cos\omega + \sin(\phi+\beta)\sin\delta}{\cos\phi\cos\delta\cos\omega + \sin\phi\sin\delta} \tag{4}$$

The estimated solar energy for inclined surfaces must be multiplied by absorbance and transmittance materials' factors in order to calculate the total energy that will be retained by the glass and absorber plate. Therefore, solar radiation absorbed by the glass and by the absorbing plate is S_1 and S_2, respectively, as described in Eqs. (5a,5b).

$$S_1 = \alpha_g I_t \tag{5a}$$

$$S_2 = \alpha_w \tau_g I_t \tag{5b}$$

where α_g is the glass absorptance, α_w is the absorber plate absorptance and τ_g is the glass transmissivity. In this study, it was considered $\tau_g = 0,84$, $\alpha_g = 0,06$, and $\alpha_w = 0,95$ as suggested by Mathur *et al.* (2006b).

2.2 Balance energy

The dimensions adopted for the solar chimney are $4\times0.1724\times0.145\ m$, with inlet and outlet areas equals to 0,025 m^2, similar values used by Ong (2003). Positioned on the ceiling level of the accommodation, the absorber plate has a thermal insulation thickness of $0.022\ m$ which is in contact with the external environment.

Figure 2 represents the resistance diagram of the solar chimney. The glass receives the solar energy S_1, where part of it is reflected back to the outside environment at temperature T_a, and another part is lost by convection due to the external wind. The absorber plate receives the energy transmitted by the glass S_2, losing a part of it due to external wind through the thermal insulation. Another part is also lost due to the radiation energy that heats the glass. Both the glass and the plate heats the air inside the channel, resulting in natural convection that starts the airflow within the chimney.

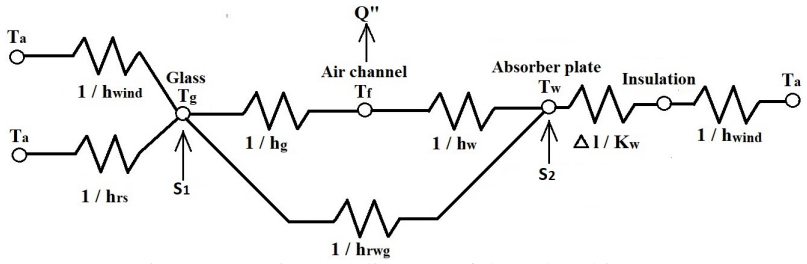

Figure 2: Resistance diagram of the solar chimney.

Thus, the energy balance around the glass can be written as follow:

$$S_1 A_g + h_{rwg} A_w (T_w - T_g) = h_g A_g (T_g - T_f) + A_g \sum Q_l \tag{6}$$

where T_g is the glass temperature, h_g is the heat transfer coefficient of air from the inner side of the glass, A_g is the glass area, A_w is the absorber plate area, T_w is the absorber plate temperature, T_f is the mean temperature of the air in the channel, and h_{rwg} is the heat transfer coefficient between the wall and the absorber plate. $\sum Q_l$ is the energy losses given by:

$$\sum Q_l = q_{wind} + q_{rs} = (h_{wind} + h_{rs})(T_g - T_a) = U_t (T_g - T_a) \tag{7}$$

where h_{wind} is the convective heat transfer coefficient, and h_{rs} is the radiative heat transfer coefficient. h_{wind} is given by Jürges *Apud* Duffie and Beckman (2013) in Eq. (8) and is dependent on wind velocity U.

$$h_{wind} = \begin{cases} 5,6 + 3,9U & \text{U<5 m/s} \\ 7,2U^{0,78} & \text{U} \geq \text{5 m/s} \end{cases} \tag{8}$$

To calculate h_{rwg} and h_{rs}, Eq. (9) and Eq. (10) are employed respectively. Both equations are given by Kalogirou (2013), where ε_g is the glass emissivity, ε_w is the absorber plate emissivity, and σ is the Stefan Boltzmann constant. In this study, it was considered $\varepsilon_g = 0.90$ and $\varepsilon_w = 0.95$.

$$h_{rs} = \varepsilon_g \sigma (T_g + T_a)(T_g^2 + T_a^2) \tag{9}$$

$$h_{rwg} = \frac{\sigma (T_w + T_g)(T_w^2 + T_g^2)}{\frac{1}{\varepsilon_w} + \frac{1}{\varepsilon_g} - 1} \tag{10}$$

The energy balance around the absorber plate can be written as follow:

$$S_2 A_w - h_{rwg} A_w (T_w - T_g) = h_w A_w (T_w - T_f) + U_b A_w (T_w - T_r) \tag{11}$$

where T_r is the room temperature and U_b is the global heat transfer coefficient through the thermal insulation layer, shown in Eq. (12). In order to simplify the problem, the room to be ventilated was considered to be insulated. So, in this work, T_r is essentially the external temperature T_a. Furthermore, conduction and convection heat losses in the thermal insulation were also considered. The thermal conductivity value of the insulation k_w is $0,0275\ W/m\ K$, as suggested by Ong (2003).

$$U_b = \frac{1}{\frac{1}{h_{wind}} + \frac{\Delta_w}{k_w}} \tag{12}$$

Both the glass and the plate provide energy to heat the air within the channel. The air heat gain q" can be expressed as:

$$q" = h_g A_g (T_g - T_f) + h_w A_w (T_w - T_f) \tag{13}$$

where h_w is the heat transfer coefficient between the air and the absorber. As noted by Hirunlabh *et al.* (1999), another expression to q" is shown in Eq. (14) and will be useful to evaluate the overall solution.

$$q" = \frac{\dot{m} c_p (T_f - T_r)}{\gamma W L} = M (T_f - T_r) \tag{14}$$

where $\dot{m}$ is the outlet mass flow rate, c_p is the specific heat coefficient, T_f is the mean temperature, and WL is the inlet section area. Lastly, $\dot{m}$ due to the stack effect can also be written according to Andersen (2003) in Eq. (15).

$$\dot{m} = c_d \rho A_o \sqrt{\frac{2gL \sin\theta (T_f - T_r)}{(1 + \frac{T_r}{T_f}(\frac{A_o}{A_i})^2) T_r}} \tag{15}$$

where c_d is the discharge coefficient for the outlet section , ρ is the air density, A_o is the outlet area, A_i is the inlet area, and g is the gravity.

The discharge coefficient c_d is an empirical value and corresponds to the ratio between theoretical and actual mass flow on discharge and is also described as in Eq.(16), where $\sum h_l$ is the head loss' system.

$$c_d = \frac{1}{\sqrt{\sum h_l}} \tag{16}$$

The head loss equation is show on Eq.(17), where $\sum l_{in}$ is the inlet losses, $\sum l_{out}$ is the outlet losses and $f\frac{L}{D_h}$ the friction loss.

$$\sum h_l = \sum l_{in} + \sum l_{out} + f\frac{L}{D_h} \tag{17}$$

According to Ortega (2011) the inlet loss coefficient could be assumed equals to $0,5$, the outlet loss coefficient equals to 1 and the roughness value is equal to $0,5$. By moody's diagram, the friction factor will be a value between 0,025 and

0,05. So, the head loss will range from $2,13 < \sum h_l < 2,77$ and consequently the discharge coefficient will be varying between $0,60$ and $0,685$.

Others authors, like de Oliveira Neves and da Silva (2018), studied others factors that could be changing the c_d value. For example, the wind direction can significantly change discharge coefficient, as shown by de Oliveira Neves and da Silva (2018), which found a variation between 0.56 and 0.8 according to the wind direction. For a vertical solar chimney, Zha *et al.* (2017) led an experiment where the results suggested 0,51 for c_d value. Although the database used in this work provides the wind speed and direction, the wind does not behave as a constant parameter throughout a city and the solar chimney can be easily affected by topography, surrounding buildings, vegetation and it's own geometry and materials. So, in this study, it was decided to adopt a fixed value for the discharge coefficient as suggested by Flourentzou *et al.* (1998), with $c_d = 0.6$.

Eqs. (6), (11) and (13) can be rearranged into a linear system and solved by Gauss-Jacobi method. The iterative process has been set to stop if the calculated values of T_f, between two successive iterations, becomes less than a preset tolerance ϵ, defined as $\epsilon = 0.001K$ for this case. Since the surface areas are the same, the equation system are shown in Eq. (18).

$$\begin{cases} T_w = (S_2 + U_b T_r + h_{rwg} T_g + h_w T_f)/(h_w + h_{rwg} + U_b) \\ T_g = (h_g T_f + h_{rwg} T_w + S_1 + U_t T_a)/(h_g + h_{rwg} + U_t) \\ T_f = (M T_r + h_g T_g + h_w T_w)/(h_g + h_w + M) \end{cases} \tag{18}$$

The system efficiency η is determined by Eq.(19), where T_s is the temperature of the air exiting the chimney, which can be calculated by Hirunlabh *et al.* (1999) proportion.

$$\eta = \frac{\dot{m} c_p (T_s - T_r)}{W L \; I_t} \tag{19}$$

2.3 Thermal properties of air

The measurements collected from weather stations also provided air relative humidity (Φ) data. So, by using Tetens equations, noted by Weiss (1977), the air density within the channel can be expressed as presented in Eq. (20), where P_{abs} is the absolute pressure, and ϕ is the relative humidity.

$$\rho = \frac{P_{abs} - (610,8 e^{\frac{17,3T_f}{237,3+T_f}}) * \phi}{287,058 T_f} + \frac{(610,8 e^{\frac{17,3T}{237,3+T_f}}) * \Phi}{461,495 T_f} \tag{20}$$

The specific heat is suggested by Asano (2007), as follows in Eq. (21), where T_m is the mean temperature between the air and surface and must be calculated for glass and absorber plate.

$$c_p = \frac{(28,11 + 1,97 T_m \times 10^{-3} + 4,8 T_m^2 \times 10^{-6} - 1,97 T_m^3 \times 10^{-9})}{28,97 \times 10^{-3}} \tag{21}$$

The Nusselt number considered is given by Vliet and Ross (1975) in Eq. (22), where the transition between laminar and turbulent regimes can be specified according to the channel inclination, with $R_a \approx 10^8$ for $\beta = 10°$ and $R_a \approx 10^{10}$ for $\beta = 90°$ as an example.

$$Nu = \begin{cases} 0,55 (G_r P_r)^{0,2} & \text{laminar} \\ 0,17 (G_r P_r)^{0,25} & \text{Turbulent} \end{cases} \tag{22}$$

where G_r is the modified Grashof number, shown in Eq. (23). G_r can be defined as a function of the Prandtl number P_r, a given hydraulic diameter D, the gravity g, an expansion coefficient β_t, a thermal conductivity coefficient k and a kinematic air viscosity ν.

$$G_r = \frac{I_t D^4 g \beta_t}{\nu^2 k} \tag{23}$$

By using the power law, the viscosity of air can be expressed as in Eq. (24) and ν can be obtained by the ratio between μ and the air density ρ.

$$\frac{\mu}{\mu_0} = (\frac{T_m}{T_0})^{0,7} \tag{24}$$

For the air thermal conductivity calculation, the expression proposed by Kannuluik and Carman (1951) is adopted in Eq. (25) with a conversion factor to SI unit included.

$$k = (5,75 \times 10^{-5}(1 + 0,00317T_m - 0,0000021T_m^2)) \times 418,4 \tag{25}$$

3. Results and discussion

Since the cities of Rio de Janeiro and Seropédica are geographically close to each other, the data analyzed proved to be very close, with slight variations between one station and another. Therefore, for practical purposes, all the results presented in this section were obtained through an average of the data from each weather station listed in Tab. 1.

Looking at Fig. 3 and Fig. 4 it can be seen that the heat absorber plate and the glass presents higher temperatures for tilts between $10°$ and $40°$ indeed. At first, this would imply a higher temperature gradient between the chimney's wall and the air within it, thus generating a higher airflow. In fact, as can be seen in Fig. 5 the difference between fluid temperature T_f and room temperature T_r is higher for lower tilt angles. However, the flow is also dependent on chimney tilt angle θ (Eq. (15)), which means being dependent on the vertical distance between the air inlet and outlet, the stack height. Therefore, to guarantee the maximum possible flow to the system, it is necessary to assess the influence that each of these variables will have on the final result.

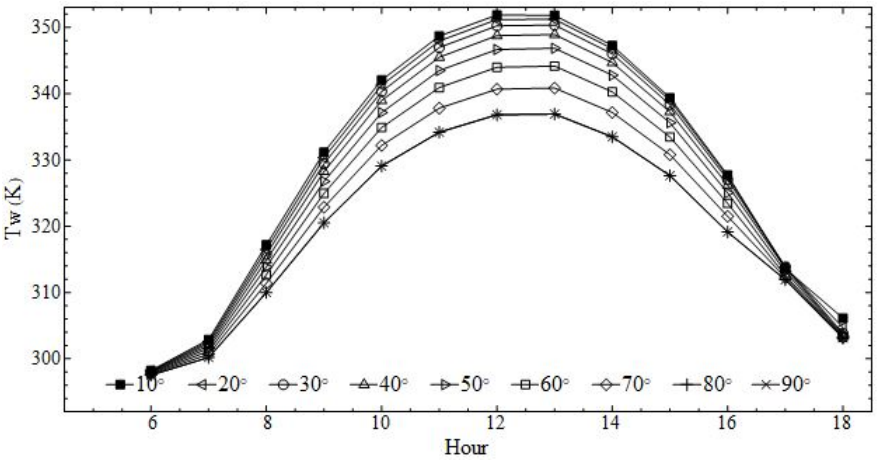

Figure 3: Average temperature of the absorbent plate during the day according to tilt angle.

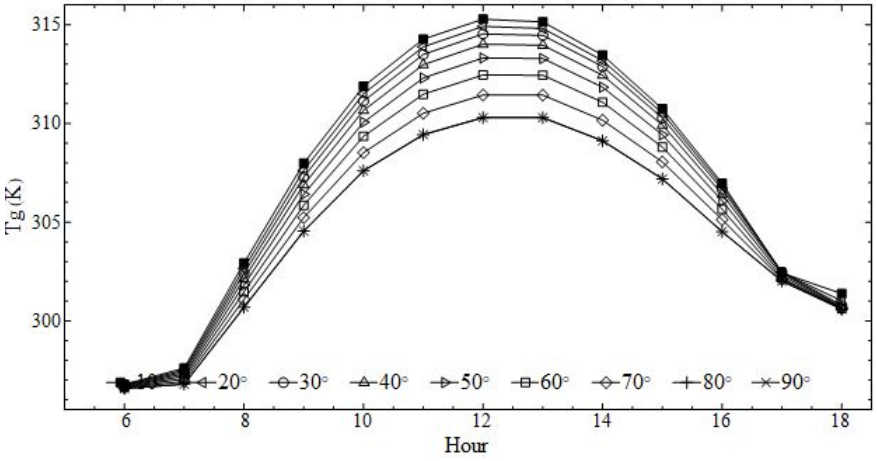

Figure 4: Average glass temperature during the day according to tilt angle.

Kalogirou (2003) argues that the optimum tilt angle for solar collectors is equal to a range of $\pm 10°$ from Latitude location. So, to Rio de Janeiro and Seropédica, located at the Latitudes shown in Tab. 1, it is expected that inclinations

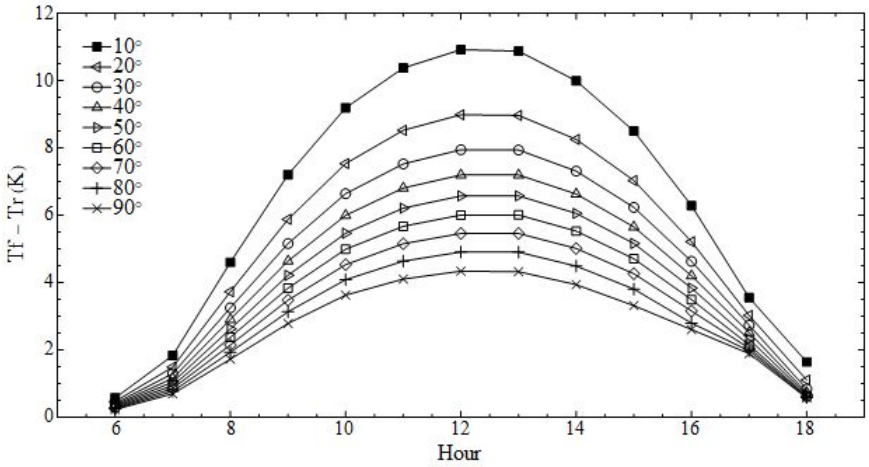

Figure 5: Average ΔT of the air within the channel during the day according to tilt angle.

close $10°$ or $30°$ benefits the energy gain. However, not necessarily this range will provide the highest air flows to a solar chimney. In Fig. 6 the average mass airflow for nine tilted chimney conditions is presented. As expected, the airflow increases from sunrise to noon and it decreases from noon until the sunset. The maximum average mass airflow obtained was 0.0138 kg/s at noon with a $60°$ tilt angle, which also guarantees the highest airflow over practically the entire period of the day with sunlight. It is also possible to notice that angles between $50°$ and $80°$, which can be considered a relatively large variation for the solar chimney tilt, the average mass airflow generated is not significantly changed. At noon, for example, the maximum airflow variation for those angles were less than 4 %. However, for tilt angles below $40°$, there is a considerable decrease in the airflow, indicating that this tilt range should not be applied in solar chimneys located in these two cities.

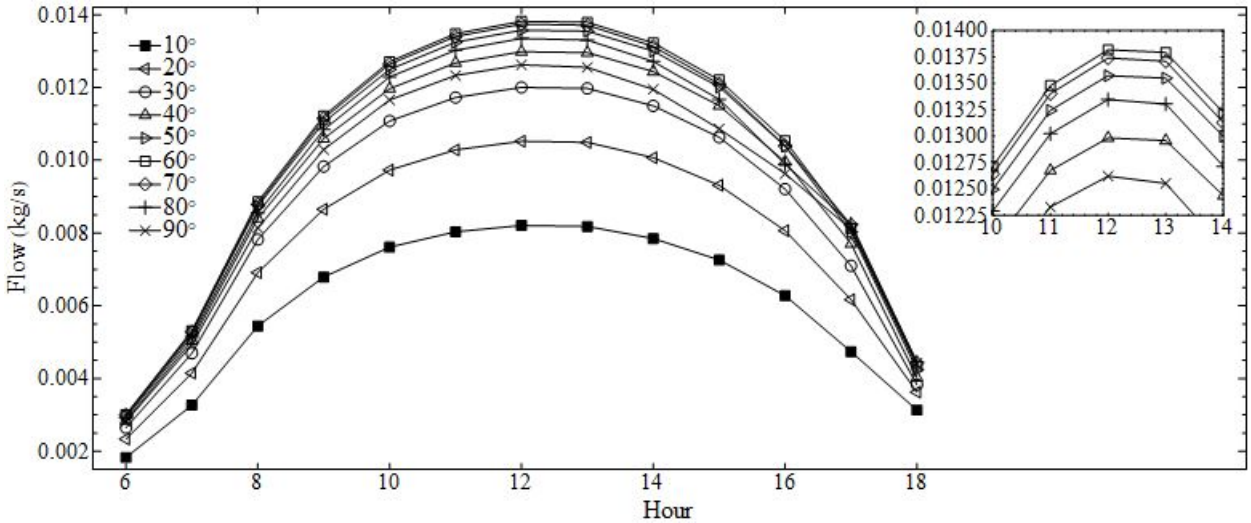

Figure 6: Average mass airflow for each hour according to tilt angle.

Throughout the year the solar energy intensity presents a natural seasonal variation. So, to evaluate the best chimney inclination during the year, the average airflow for each month were calculated and are presented in Fig. 7. These data show similarities with those presented in Fig. 6, with the higher average airflow being achieved for tilt angles between $50°$ and $70°$, depending on the month analyzed, which are close to the tilt angles found by Bassiouny and Korah (2009) and Sakonidou *et al.* (2008). However, the month that generated the highest average airflow was April, instead of a month during summer period. Although it appears to be contradictory, there is a reasonable explanation for that. The zenith angle has a huge impact on the energy captured by the absorber plate, as can be seen in Fig. 8. A low zenith angle means that the ecliptic is substantially parallel to a vertical chimney, thereby reducing the solar radiation that reaches the absorber plate and, consequently, reducing the energy transferred to the air within the channel. In summer the zenith angle is lower than in winter. So, for higher tilt angles the absorber plate capture less energy in summer than in winter. The opposite is true for lower tilt angles. As an example, for a $60°$ tilt, the solar radiation reaching the system is higher in April than any summer month, resulting in higher airflow in this month with this tilt.

Besides that, it is important to notice that the airflow results were computed based on the hourly weather measurements

from INMET. However, summer has longer days in comparison to winter, which means that the solar chimney can be active more hours during a summer day. Instead of calculating only the average airflow in kg/s, Fig. 9 shows the average airflow in kg/day for each month of the year, giving more reliable information about the chimney airflow. Therefore, despite the average airflow, presented in 9, shows higher values in April, the daily average airflow is higher in January as would be expected. Table 2 shows the same data but as an average for each season of the year. As expected, during the summer period, higher daily average airflow values are obtained in comparison with other seasons. Also, in summer, one can observe a performance reduction of the chimney in the vertical condition due to the low zenith angle, generating airflow similar to $20°$ and $30°$ tilt. Indeed, when comparing the results for the chimney with a $10°$ and $90°$ inclination, it is clear that the stack height has a greater influence on the airflow result than the solar radiation reaching the system.

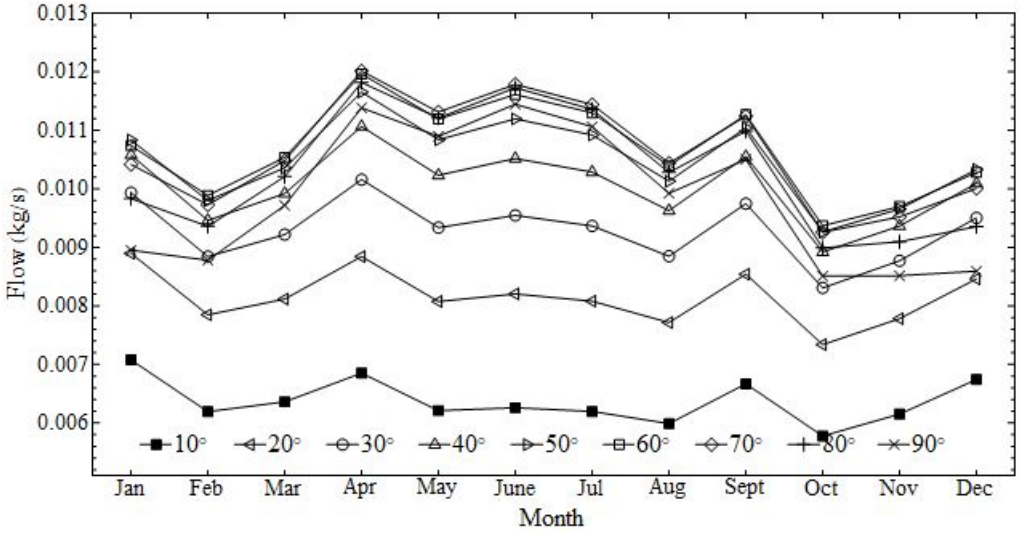

Figure 7: Average mass airflow (kg/s) for each month according to the tilt angle.

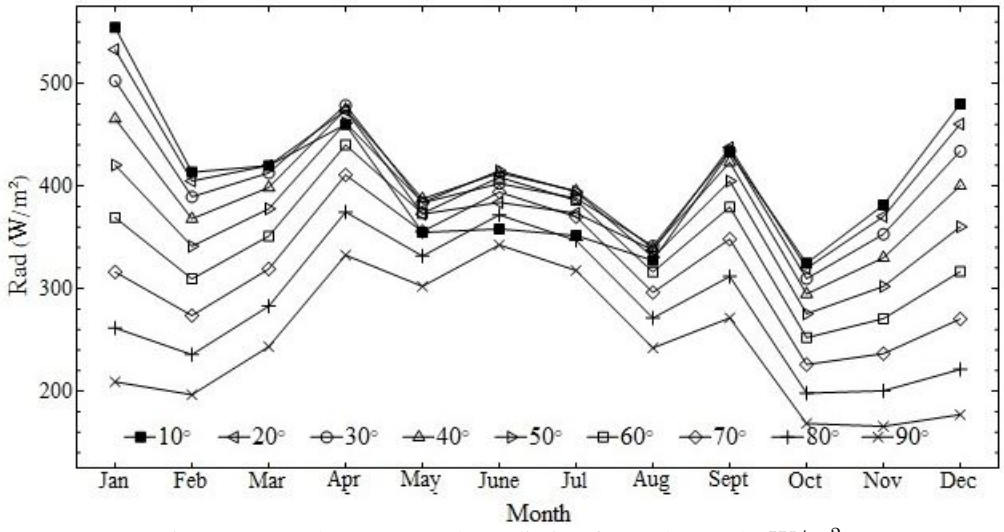

Figure 8: Hourly average solar radiation for each month (W/m^2)

Therefore, it is possible to state that, in the two cities under study, there is no need to implement an automatic system to control the chimney tilt, either during the day or throughout the year. In both cases, angles between $60°$ and $70°$ already guarantee the highest flow rates, with minimal differences between then.

The chimney efficiency was also computed. Fig. 10 presents the average efficiency for each hour and different tilt angles considered so far, where is possible do see the efficiency behaving almost the same way as the airflow, i.e., increasing from sunrise until 11-12 a.m. and then decreasing. The maximum average efficiency obtained was 0.343 at 11 a.m. with $50°$ tilt, a little bit higher than the case with $60°$ tilt. In Fig. 11 the average efficiencies for each month are presented, and as can be verified, the higher efficiencies were obtained during Autumn and Winter seasons, since the average airflow (Fig. 7) also increase during this period, with the highest efficiency happening in April. As explained before, the main reason for that is the low zenith angle in the two cities of interest during summer.

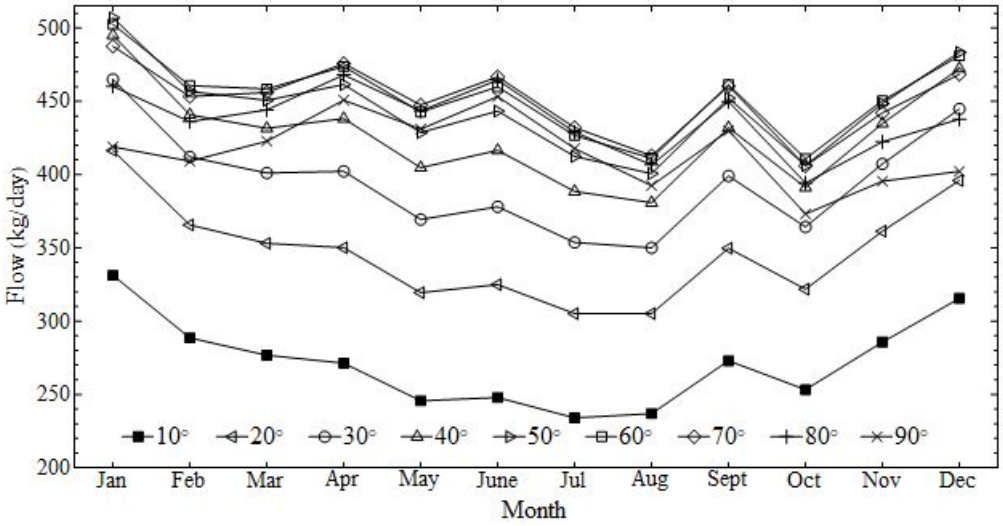

Figure 9: Daily average mass airflow (kg/day) for each month according to the tilt angle.

Inclination	10°	20°	30°	40°	50°	60°	70°	80°	90°
Summer	298.86	378.40	425.99	455.82	471.47	473.88	465.60	446.79	416.93
Autumn	254.94	331.50	383.21	419.80	444.50	458.74	463.28	458.61	445.01
Winter	247.95	320.01	367.59	400.42	421.74	433.03	435.10	428.45	413.40
Spring	284.82	359.72	405.45	432.81	446.04	447.43	438.82	418.14	390.24

Table 2: Daily average mass airflow (kg/day) for each season according to tilt angle

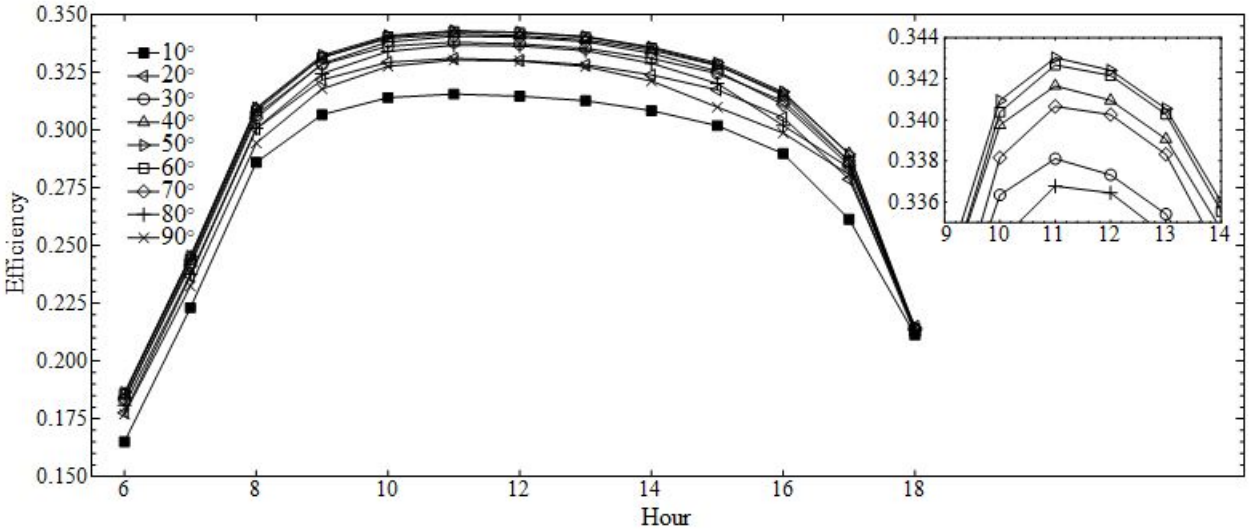

Figure 10: Hourly average efficiency of the solar chimney according to the tilt angle.

4. Conclusions

The present study aimed to calculate an optimal tilt range for a solar chimney to generate the maximum possible airflow in Rio de Janeiro and Seropédica cities. This goal was achieved by using the hourly weather measurements from INMET to do all the calculations necessary. The results showed that the highest airflow were obtained with a tilt angle between 60° and 70° regardless of the time or month analyzed. Therefore, implement an automatic system to control the chimney tilt, like the ones installed in a photovoltaic system, should not present a good cost-benefit. Also, we verified that the chimney stack height has a greater impact on the system airflow than the solar radiation that reaches the absorber plate.

It is worth mentioning that the weather data considered for this study covers only one year of measurements, and may not be enough to have a better estimate of the airflow results. More complex and seasonal climatic phenomena, such as El Nino, may not have been captured in this study, requiring more data to be analyzed.

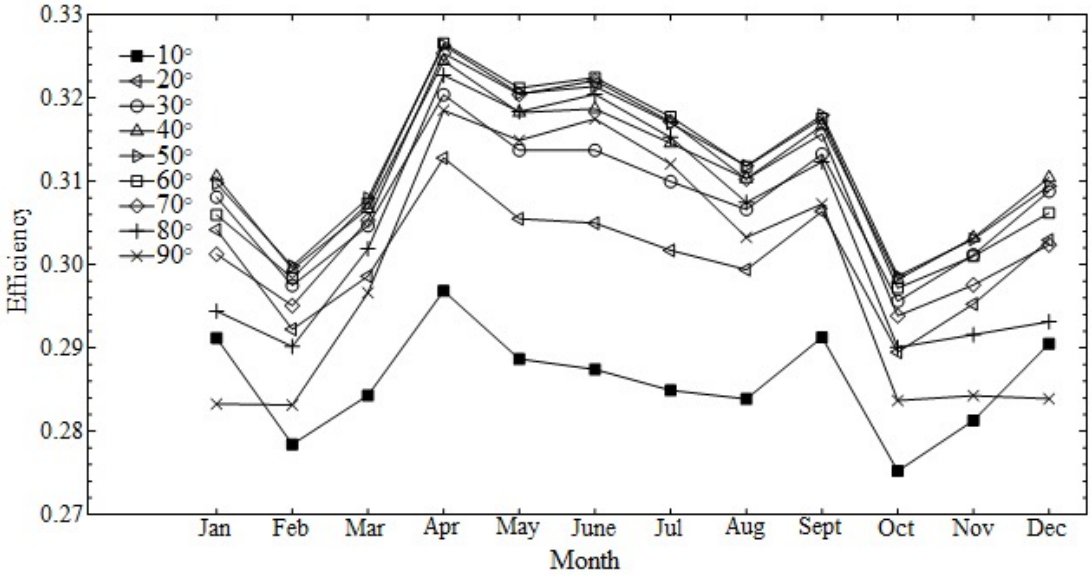

Figure 11: Hourly average efficiency of the solar chimney for each month according to the tilt angle.

5. REFERENCES

Andersen, K.T., 2003. "Theory for natural ventilation by thermal buoyancy in one zone with uniform temperature". *Building and Environment*, Vol. 38, No. 11, pp. 1281–1289.

Asano, K., 2007. *Mass Transfer: From fundamentals to modern industrial applications*. John Wiley & Sons.

Bassiouny, R. and Korah, N.S., 2009. "Effect of solar chimney inclination angle on space flow pattern and ventilation rate". *Energy and Buildings*, Vol. 41, No. 2, pp. 190–196.

Chen, Z.D., Bandopadhayay, P., Halldorsson, J., Byrjalsen, C., Heiselberg, P. and Li, Y., 2003. "An experimental investigation of a solar chimney model with uniform wall heat flux". *Building and Environment*, Vol. 38, No. 7, pp. 893–906.

Clezar, C.A. and Nogueira, A.C.R., 1999. *Ventilação industrial*. Editora da UFSC.

de Oliveira Neves, L. and da Silva, F.M., 2018. "Simulation and measurements of wind interference on a solar chimney performance". *Journal of Wind Engineering and Industrial Aerodynamics*, Vol. 179, pp. 135–145.

Duffie, J.A. and Beckman, W.A., 2013. *Solar engineering of thermal processes*. John Wiley & Sons.

Erbs, D., Klein, S. and Duffie, J., 1982. "Estimation of the diffuse radiation fraction for hourly, daily and monthly-average global radiation". *Solar energy*, Vol. 28, No. 4, pp. 293–302.

Flourentzou, F., Van der Maas, J. and Roulet, C.A., 1998. "Natural ventilation for passive cooling: measurement of discharge coefficients". *Energy and buildings*, Vol. 27, No. 3, pp. 283–292.

Freixanet, F., Armando, V. and Manuel, R.V., 2004. *Ventilación natural: cálculos básicos para arquitectura*. Universidad Autónoma Metropolitana, Unidad Azcapotzalco, Rectoría de Unidad .

Hirunlabh, J., Kongduang, W., Namprakai, P. and Khedari, J., 1999. "Study of natural ventilation of houses by a metallic solar wall under tropical climate". *Renewable Energy*, Vol. 18, No. 1, pp. 109–119.

Hung, T.C., Huang, T.J., Lee, D.S., Lin, C.H., Pei, B.S. and Li, Z.Y., 2017. "Numerical analysis and experimental validation of heat transfer characteristic for flat-plate solar air collector". *Applied Thermal Engineering*, Vol. 111, pp. 1025–1038.

INMET, 2019. "Estação meteorológica de observação de superfície automática". URL `http://www.inmet.gov.br/portal/index.php?r=estacoes/estacoesAutomaticas`.

Jianliu, X. and Weihua, L., 2013. "Study on solar chimney used for room natural ventilation in nanjing". *Energy and Buildings*, Vol. 66, pp. 467–469.

Kalogirou, S., 2003. "The potential of solar industrial process heat applications". *Applied Energy*, Vol. 76, No. 4, pp. 337–361.

Kalogirou, S.A., 2013. *Solar energy engineering: processes and systems*. Academic Press.

Kannuluik, W. and Carman, E., 1951. "The temperature dependence of the thermal conductivity of air". *Australian Journal of Chemistry*, Vol. 4, No. 3, pp. 305–314.

Mathur, J., Bansal, N., Mathur, S., Jain, M. *et al.*, 2006a. "Experimental investigations on solar chimney for room ventilation". *Solar Energy*, Vol. 80, No. 8, pp. 927–935.

Mathur, J., Mathur, S. *et al.*, 2006b. "Summer-performance of inclined roof solar chimney for natural ventilation". *Energy*

and Buildings, Vol. 38, No. 10, pp. 1156–1163.

Muneer, T., 2007. *Solar radiation and daylight models*. Routledge.

Ong, K., 2003. "A mathematical model of a solar chimney". *Renewable energy*, Vol. 28, No. 7, pp. 1047–1060.

Ortega, E.P., 2011. "Analyzes of solar chimney design". *Master's Thesis submitted to the Norwegian University of Science and Technology, Department of Energy and Process Engineering July*.

Sakonidou, E., Karapantsios, T., Balouktsis, A. and Chassapis, D., 2008. "Modeling of the optimum tilt of a solar chimney for maximum air flow". *Solar Energy*, Vol. 82, No. 1, pp. 80–94.

Vliet, G. and Ross, D., 1975. "Turbulent natural convection on upward and downward facing inclined constant heat flux surfaces". *Journal of Heat Transfer*, Vol. 97, No. 4, pp. 549–554.

Weiss, A., 1977. "Algorithms for the calculation of moist air properties on a hand calculator". *Transactions of the ASAE*, Vol. 20, No. 6, pp. 1133–1136.

Zha, X., Zhang, J. and Qin, M., 2017. "Experimental and numerical studies of solar chimney for ventilation in low energy buildings". *Procedia Engineering*, Vol. 205, pp. 1612–1619.

6. RESPONSIBILITY NOTICE

The authors are solely responsible for the printed material included in this paper.